Above-threshold detachment by strong ultrashort two-component laser pulses

D. Habibović [1] and D. B. Milošević [1,2]

[1] *University of Sarajevo, Faculty of Science, Zmaja od Bosne 35, 71000 Sarajevo, Bosnia and Herzegovina*

[2] *Academy of Sciences and Arts of Bosnia and Herzegovina, Bistrik 7, 71000 Sarajevo, Bosnia and Herzegovina*

(Received 23 March 2023; accepted 2 May 2023; published 15 May 2023)

Detachment of electrons from negative ions by the ultrashort few-cycle laser pulses in the near-infrared spectral region is investigated using a theory based on the strong-field approximation. The differential detachment probability is computed by the numerical integration or by using the saddle-point method. The symmetry properties of the photoelectron momentum distribution are analyzed for the elliptically polarized as well as for the bi-elliptical driving field with the sine-square pulse envelope and compared with those obtained using a long pulse with a flat envelope. We show that the differential detachment probability depends, to a significant extent, on the polarization state of the driving light. For the direct electrons, i.e., the electrons which, after the detachment, do not interact with the parent atom, this is not the case if the process is induced by a long pulse with a flat envelope. In addition to the polarization state, the photoelectron momentum distribution also depends on the value of the absolute phase. We show that the qualitative and quantitative characteristics of the momentum distribution can accurately be controlled using this parameter as a control knob. This control is particularly successful in the regions where the rescattered electrons are dominant due to the fact that they stay longer in the applied laser field.

DOI: 10.1103/PhysRevA.107.053110

I. INTRODUCTION

Strong-field laser-matter interaction has attracted significant attention for more than 30 years. In particular, prominent processes include above-threshold detachment (ATD), where the atomic or molecular anion is ionized by a strong laser field, and a similar process called above-threshold ionization (ATI), where a neutral atom or molecule is ionized. In both cases, the liberated electron can go directly to the detector (these are the so-called direct electrons), or it can experience additional interaction with the parent system, thus gaining a much higher energy (the so-called rescattered electrons). In the later case, these processes are denoted as high-order ATD (HATD) and high-order ATI (HATI). Besides the rescattering, it is also possible for the freed electron to recombine with the parent system, emitting the excess energy in the form of a high-energy photon. This scenario corresponds to the process called high-order harmonic generation (HHG) (for reviews about strong-field processes see Refs. [1–9]).

Advances in laser technology have made it possible to generate the ultrashort (also called few-cycle) pulses in visible, near-infrared, or midinfrared region, with a duration of only a few femtoseconds [10,11]. The intensity of the corresponding electric field is close to the intensity of the binding field of the atom or molecule, thus allowing one to explore the atomic or molecular system with excellent resolution [12]. Furthermore, the attosecond resolution can be achieved with the help of the attosecond pulses produced by an in-phase mode-locked group of subsequent high harmonics for various parts of the electromagnetic spectrum [13–16]. Additionally, the light obtained via the HHG process can be employed to access information about the structure of the system in question [17–19]. Besides the intensity and wavelength, few-cycle pulses are also characterized by the carrier-envelope phase which is sometimes called the absolute phase. This phase represents the phase difference between the maximum of the pulse envelope and the nearest maximum of the carrier wave. The influence of the absolute phase on the HHG spectra was noticed theoretically in [20]. Furthermore, using a few-cycle laser with nonstabilized absolute phase, it was shown experimentally that this parameter affects the photoionization [21]. The corresponding theoretical simulation was performed in [22]. The characteristics of the HATI and HATD processes are influenced to a great extent by this parameter, which is particularly pronounced in the high-energy part of the spectrum. There, the rescattered electrons, which stay much longer in the applied field, are dominant. The strong dependence of the rescattered electrons on the absolute phase was recognized in [23] where the asymmetry between the left- and right-emitted electrons was predicted theoretically. The experimental analysis of this asymmetry was presented in [24] using few-cycle pulses with the stabilized absolute phase (the stability of the absolute phase was achieved in [25]). The ATI experiments designed to measure the influence of the absolute phase on the photoelectron spectra are called the stereo-ATI experiments.

In recent years, bichromatic fields have attracted particular attention. In this case, the applied field consists of the two components with the same or a different envelope. For example, using two circularly polarized pulses with the same envelope and nonzero time delay, electron vortices can be successfully analyzed [26–31]. The electron vortices obtained in photodetachment of the H^- ion by one or two co or counterrotating circularly polarized ultrashort laser pulses were analyzed in [32,33] using the theory based on the strong-field approximation (SFA) or by solving the time-dependent Schrödinger equation numerically. Moreover, the positive ions

were also analyzed using the two-color few-cycle fields. For example, the ionization of He^+ was explored in [34], while in [35] the $H_2{}^+$ ion was investigated. The difference between the photoelectron energy spectra obtained with co and counterrotating bicircular field with a week second harmonic component was investigated using a semiclassical model in [36], while in [37] ATD was explored using the low-frequency approximation. Additionally, in [38], the elliptic dichroism of neutral atoms exposed to a bicircular field was analyzed through the interference of the possible ionization pathways. In the end, we mention that, in addition to ionization and rescattering, the bichromatic few-cycle pulses were also employed to explore the HHG process [39,40].

In this paper, we scrutinize HATD by the monochromatic and bichromatic elliptically polarized few-cycle pulses using the theory based on the SFA [9]. This approach assumes that the motion of the liberated electron is only governed by the applied field until eventual rescattering. For the HATI process, this means that the Coulomb interaction with the residual ion is neglected, thus leading to a disagreement of the SFA and the exact models in the low-energy part of the spectrum. However, in the HATD process, the residual system is a neutral atom so that the Coulomb effects are absent and an excellent agreement with the experiments is achieved [41]. A similar theory was employed to discuss HATD induced by a long pulse with a flat envelope for both atomic and molecular ions [42,43], while an improved version of the SFA theory and the theory based on the solution of the time-dependent Schrödinger equation were utilized in [44]. In the present contribution, we calculate the probability amplitude by the numerical integration or by using the saddle-point (SP) method. The main goal is to investigate how the photoelectron spectra depend on the helicity of the driving field and on the value of the absolute phase. Moreover, we explore the symmetry properties of the obtained momentum distributions and compare them with those obtained using a long pulse with a flat envelope. The rest of the paper is organized as follows. Section II briefly presents the SFA theory for calculating probability amplitude and gives a short description of the SP method. Additionally, the driving pulse is defined. In Sec. III numerical results obtained for the F^- ion are presented for single-color and bichromatic elliptically polarized pulses. Finally, our main conclusions and discussions are stated in Sec. IV. Atomic units are used throughout the paper.

II. THEORETICAL BACKGROUND

A. Differential detachment probability

In the framework of the SFA theory, the differential detachment probability for the transition from the ground state ψ_0 to the state with the asymptotic momentum $\mathbf{p}$ (the photoelectron energy is $E_\mathbf{p} = \mathbf{p}^2/2$) is $W_\mathbf{p} = p|M_\mathbf{p}|^2$, $p = |\mathbf{p}|$, with the probability amplitude $M_\mathbf{p} = M_\mathbf{p}^{(0)} + M_\mathbf{p}^{(1)}$, where [3]

$$M_\mathbf{p}^{(0)} = -i\int_0^{\tau_p} dt_0 \langle \tilde{\mathbf{p}} + \mathbf{A}(t_0)|\mathbf{r}\cdot\mathbf{E}(t_0)|\psi_0\rangle e^{iS(\tilde{\mathbf{p}},t_0)}, \quad (1)$$

$$M_\mathbf{p}^{(1)} = \int_0^{\tau_p} dt e^{iS(\tilde{\mathbf{p}},t)} \int_0^t dt_0 \left[\frac{2\pi}{i(t-t_0)}\right]^{3/2} \langle \tilde{\mathbf{p}}|V|\mathbf{k}_{\rm st}\rangle \times e^{-iS(\mathbf{k}_{\rm st};t,t_0)} \langle \mathbf{k}_{\rm st} + \mathbf{A}(t_0)|\mathbf{r}\cdot\mathbf{E}(t_0)|\psi_0\rangle, \quad (2)$$

are the contributions of the direct and rescattered electrons, respectively. Here $\tilde{\mathbf{p}} \equiv \mathbf{p} - \mathbf{A}(\tau_p)$, $\mathbf{k}_{\rm st} \equiv -\int_{t_0}^t dt' \mathbf{A}(t')/(t-t_0)$ is the stationary momentum, $\mathbf{A}(t)$ is the vector potential of the applied field $\mathbf{E}(t)$, τ_p is the total pulse duration, and t_0 and t are the ionization and rescattering times, respectively. Moreover, $S(\tilde{\mathbf{p}}, t_0) = I_p t_0 + \int^{t_0} dt'[\tilde{\mathbf{p}} + \mathbf{A}(t')]^2/2$ is the action of the direct electrons, while $S(\mathbf{k}_{\rm st}; t, t_0) = \int_{t_0}^t dt'\{[\mathbf{k}_{\rm st} + \mathbf{A}(t')]^2/2 + I_p\}$ is the action of the rescattered electrons and I_p is the electron affinity.

The ground-state wave function ψ_0 is represented as a linear combination of the Slater-type orbitals

$$\psi_{lm}(\mathbf{r}) = \sum_a C_a \frac{(2\zeta_a)^{n_a+1/2}}{\sqrt{(2n_a)!}} r^{n_a-1} e^{-\zeta_a r} Y_{lm}(\Omega), \quad (3)$$

where $Y_{lm}(\Omega)$ are the normalized spherical harmonics in complex form. In this paper we use the F^- ion as an example. The ground state is modeled using four $2p$ orbitals ($n_a = 2$, $l = 1$, $m = 0, \pm 1$) and the coefficients C_a and ζ_a are tabulated in [45]. For this ion, the rescattering potential can be represented by a sum of two Yukawa potentials $V(r) = (-a_1 e^{-b_1 r} - a_2 e^{-b_2 r})/r$ with the coefficients given in [44,46]. The corresponding matrix element for a single Yukawa potential is

$$\left\langle \tilde{\mathbf{p}} \middle| a\frac{e^{-br}}{r} \middle| \mathbf{k}_{\rm st} \right\rangle = \frac{a}{2\pi^2[(\tilde{\mathbf{p}} - \mathbf{k}_{\rm st})^2 + b^2]}. \quad (4)$$

The integral which appears in the amplitude $M_\mathbf{p}^{(0)}$ can be calculated either numerically or by using the SP method. In the later case, the stationarity condition $\partial S(\tilde{\mathbf{p}}, t_0)/\partial t_0 = 0$ leads to the SP equation [3]

$$[\tilde{\mathbf{p}} + \mathbf{A}(t_{0s})]^2 = -2I_p, \quad (5)$$

where the solutions t_{0s} satisfy $0 < \mathrm{Re}\, t_{0s} < \tau_p$ and $\mathrm{Im}\, t_{0s} > 0$. The direct amplitude $M_\mathbf{p}^{(0)}$ can be represented as a sum of the contributions of different SP solutions

$$M_\mathbf{p}^{(0)} \approx -i\sum_s \sqrt{\frac{2\pi i}{S_s''}} \langle \tilde{\mathbf{p}} + \mathbf{A}(t_{0s})|\mathbf{r}\cdot\mathbf{E}(t_{0s})|\psi_0\rangle e^{iS(\tilde{\mathbf{p}},t_{0s})}, \quad (6)$$

where $S_s'' = \partial^2 S(\tilde{\mathbf{p}}, t_0)/\partial t_0^2|_{t_{0s}} = -\mathbf{E}(t_{0s})\cdot[\tilde{\mathbf{p}} + \mathbf{A}(t_{0s})]$. When the SP method is employed to calculate the probability amplitude, the ground state is usually represented using the asymptotic wave functions

$$\psi_0 = \psi_{lm}(\mathbf{r}) = (A/r)e^{-\kappa r} Y_{lm}(\Omega), \quad (7)$$

where $\kappa = \sqrt{2I_p}$ and the coefficient A can be found in [47] (see also Appendix B in [48]). A similar approach can be applied to calculate the rescattering probability amplitude. The corresponding SP equations and the expression for $M_\mathbf{p}^{(1)}$ can be found in [3].

B. Electric field

In this paper we use the laser field $\mathbf{E}(t) = \mathbf{E}_1(t) + \mathbf{E}_2(t)$, where

$$\mathbf{E}_1(t) = \mathcal{E}_1 f(t)[\cos(r\omega t + \varphi_1)\hat{\mathbf{e}}_x + \varepsilon_1 \sin(r\omega t + \varphi_1)\hat{\mathbf{e}}_y],$$
$$\mathbf{E}_2(t) = \mathcal{E}_2 f(t)[\cos(s\omega t + \varphi_2)\hat{\mathbf{e}}_y + \varepsilon_2 \sin(s\omega t + \varphi_2)\hat{\mathbf{e}}_x], \quad (8)$$

$\omega = 2\pi/T$ is the fundamental frequency, T is the laser-field period, r and s are integers, $\mathcal{E}_j = E_j/\sqrt{1+\varepsilon_j^2}$, and E_j, φ_j, and ε_j, $j = 1, 2$, are the amplitudes, absolute phases, and ellipticities of the field components, respectively. The real unit vectors $\hat{\mathbf{e}}_x$ and $\hat{\mathbf{e}}_y$ define the pulse polarization plane. We choose the sine-square pulse envelope, i.e., $f(t) = \sin^2(\omega_p t/2)$, $\omega_p = \omega/n_p$, where n_p is the integer number of optical cycles in the pulse so that the pulse length is $\tau_p = n_p T$. The vector potential, which corresponds to the field $\mathbf{E}(t)$, can be written as $\mathbf{A}(t) = \mathbf{A}_1(t) + \mathbf{A}_2(t)$, where

$$\mathbf{A}_1(t) = \sum_{i=1}^{3} \mathcal{A}_i[\varepsilon_1 \cos(\omega_i t + \varphi_1)\hat{\mathbf{e}}_y - \sin(\omega_i t + \varphi_1)\hat{\mathbf{e}}_x],$$

$$\mathbf{A}_2(t) = \sum_{i=4}^{6} \mathcal{A}_i[\varepsilon_2 \cos(\omega_i t + \varphi_2)\hat{\mathbf{e}}_x - \sin(\omega_i t + \varphi_2)\hat{\mathbf{e}}_y], \quad (9)$$

$\mathcal{A}_1 = \mathcal{E}_1/(2\omega_1)$, $\mathcal{A}_4 = \mathcal{E}_2/(2\omega_4)$, $\mathcal{A}_i = -\mathcal{E}_1/(4\omega_i)$, $i = 2, 3$, $\mathcal{A}_j = -\mathcal{E}_2/(4\omega_j)$, $j = 5, 6$, and $\omega_1 = r\omega$, $\omega_2 = r\omega + \omega_p$, $\omega_3 = r\omega - \omega_p$, $\omega_4 = s\omega$, $\omega_5 = s\omega + \omega_p$, $\omega_6 = s\omega - \omega_p$. To quantify the difference between the spectra obtained using the pulses with the component ellipticities ε_j and $-\varepsilon_j$, $j = 1, 2$, we use the elliptic-dichroism parameter [49]

$$\delta_{\mathbf{p}}(\varepsilon_1, \varepsilon_2) = \frac{W_{\mathbf{p}}(\varepsilon_1, \varepsilon_2) - W_{\mathbf{p}}(-\varepsilon_1, -\varepsilon_2)}{W_{\mathbf{p}}(\varepsilon_1, \varepsilon_2) + W_{\mathbf{p}}(-\varepsilon_1, -\varepsilon_2)}, \quad (10)$$

which represents the normalized difference between the differential detachment probability calculated with ε_j and $-\varepsilon_j$, $j = 1, 2$, respectively. If $\varepsilon_1 = \varepsilon_2 = \varepsilon$, we denote $\delta_{\mathbf{p}}(\varepsilon_1, \varepsilon_2) \equiv \delta_{\mathbf{p}}(\varepsilon)$.

III. NUMERICAL RESULTS

We present our numerical results using the example of the F^- ion exposed to various two-component fields. The electron affinity of the F^- ion is $I_p = 3.4$ eV. For this target, due to the short range of the binding potential, the detachment process can be reliably described using the SFA. This is not the case for neutral targets for which the long-range Coulomb interaction of the parent positive ion and the electron strongly affects the low-energy part of the spectrum. We define the emission direction of the photoelectrons by the emission angle θ_e, which is the angle between the final photoelectron momentum and the positive p_x axis. Pulse duration τ is defined by the full width at half maximum (FWHM) of the intensity. In our case it is $\tau = 0.36406\tau_p$ [3]. In all examples, we use the few-cycle pulse with the sine-square envelope, $n_p = 4$, and $\lambda = 2000$ nm. This corresponds to a pulse with the duration $\tau = 9.71$ fs. The energy of the photon of the fundamental component of the pulse is 0.62 eV, i.e., it is more than five times smaller than the electron affinity of the F^- ion.

A. Elliptically polarized field

First, we explore the case of an elliptically polarized few-cycle pulse, i.e., $\mathbf{E}(t) = \mathbf{E}_1(t)$. In Fig. 1 we present the logarithm of the differential detachment probability in the pulse polarization plane for the F^- ion exposed to the four-cycle elliptically polarized field with the intensity $I = E_1^2 = 1.5 \times 10^{13}$ W/cm^2, the wavelength of 2000 nm, and the ellipticity $\varepsilon = \varepsilon_1 = 0.2$. The absolute phase is $\varphi_1 = 0°$. Both the direct and rescattered electrons are taken into consideration.

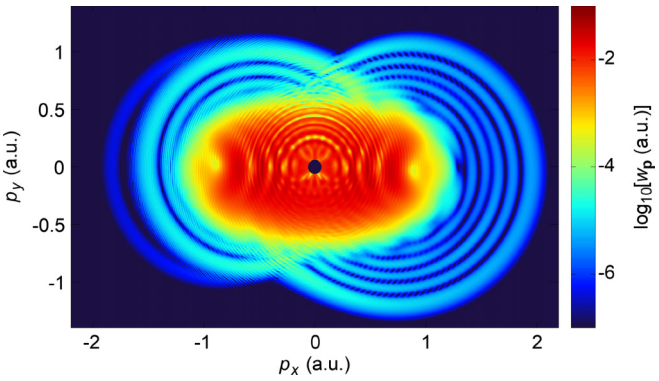

FIG. 1. Logarithm of the differential detachment probability in the pulse polarization plane for the F^- ion exposed to the four-cycle elliptically polarized field with the intensity $I = E_1^2 = 1.5 \times 10^{13}$ W/cm^2, the wavelength of 2000 nm, and the ellipticity $\varepsilon = \varepsilon_1 = 0.2$. The absolute phase is $\varphi_1 = 0°$. Both the direct and rescattered electrons are taken into consideration.

The symmetry properties of the photoelectron momentum distribution are closely related to the symmetry properties of the applied field and the corresponding vector potential [50]. In particular, the vector potential can exhibit various rotational symmetries which preserve the direction of the time evolution, as well as the reflection symmetries for which the time evolution is reversed. As a consequence, the first type of symmetry property is directly imprinted onto the momentum distribution, while the second type is mapped only onto the part of the spectrum which corresponds to the direct electrons. For a long elliptically polarized pulse with a flat envelope, the electric field and the corresponding vector potential are invariant with respect to the rotation by the angle π around the axis which is perpendicular to the pulse polarization plane, so that the momentum distribution possesses the same symmetry. In our case of an ultrashort elliptically polarized pulse, this symmetry is broken. This can easily be checked by performing the time translation $t \to t + \tau_p/2$ and calculating $\mathbf{E}_1(t + \tau_p/2)$ which differs from $\mathbf{E}_1(t)$ by more than a sign. As a consequence, the applied field, the corresponding vector potential, and the differential detachment probability are not invariant with respect to the rotation by the angle π around the p_z axis, and the asymmetry between the left and right lobes in Fig. 1 is well pronounced.

Let us now investigate what happens with the differential detachment probability when the ellipticity of the driving field changes the sign. In Fig. 2 we present the elliptic-dichroism parameter, Eq. (4), which corresponds to the photoelectron momentum distributions of the F^- ion exposed to the laser field with the ellipticity $\varepsilon = \pm 0.2$ and the other parameters the same as in Fig. 1. The spectrum shown in Fig. 1 is obtained for the field ellipticity $\varepsilon = 0.2$, while the spectrum for $\varepsilon = -0.2$ is obtained from the one shown in Fig. 1 by the reflection with respect to the p_x axis. The elliptic-dichroism parameter is not zero because the spectrum itself does not exhibit the reflection symmetry with respect to the p_x axis. At the center of the pulse polarization plane, the contribution of the direct electrons is dominant, while the lobe structures correspond to the

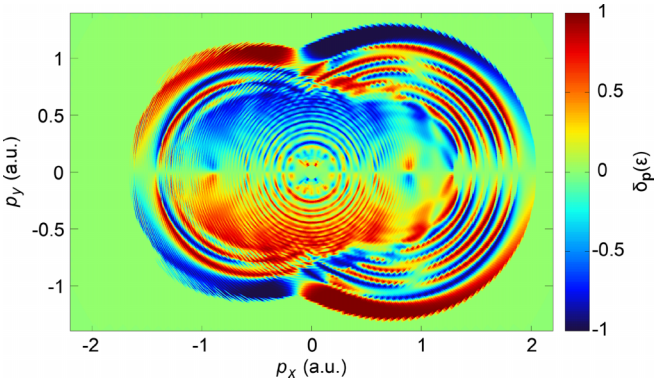

FIG. 2. The elliptic-dichroism parameter for the F^- ion exposed to the field with the ellipticity $\varepsilon = \pm 0.2$ and other parameters the same as in Fig. 1. Both the direct and rescattered electrons are taken into consideration.

rescattered electrons. For a given direction of the photoelectron emission, the elliptic-dichroism parameter for the rescattered electrons as a function of the photoelectron energy exhibits rapid oscillations between the extremal values $\delta_{\mathbf{p}}(\varepsilon) = \pm 1$. This is particularly pronounced in the region $p_x > 0$ where the length of the rescattering plateau is longer. The electrons with the highest energy can appear for different values of the photoelectron momentum components, depending on the value of the absolute phase φ_1. Additionally, it is important to remind ourselves that the differential detachment probability of the rescattered electrons decreases significantly with the increase of the ellipticity of the applied field so that much larger values of the field ellipticity are not interesting.

The direct electrons deserve particular attention. For a long pulse with a flat envelope, the time inversion $t \to -t$ leads to the reflection of the vector potential with respect to the y axis, which, together with the earlier discussed rotational symmetry, induces the four-fold symmetry of the momentum distribution. Additionally, the change of the sign of the applied-field ellipticity induces the reflection of the vector potential with respect to the x axis without affecting the spectra. As the result, the elliptic-dichroism parameter is zero (see Fig. 3 in [49]). This means that the direct electrons, for which the differential detachment probability is much higher than that of the rescattered electrons, are not sensitive to the helicity of the driving field. The situation is substantially different if an ultrashort pulse is employed as a driving field. In Fig. 3 we present the logarithm of the differential detachment probability of the direct electrons for the F^- ion exposed to an elliptically polarized field with the ellipticity $\varepsilon = 0.2$ (left panel) and $\varepsilon = -0.2$ (middle panel). For a long driving pulse with a flat envelope, the switch of the helicity of the driving field leads to the reflection $p_y \to -p_y$. However, for an ultrashort pulse, this transformation changes the spectrum, i.e., the momentum distributions obtained for $\varepsilon = 0.2$ and $\varepsilon = -0.2$ are not the same (cf. the left and middle panels of Fig. 3). The difference between these two distributions is quantified using the elliptic-dichroism parameter (see the right panel of Fig. 3). On average, in the region $p_y > 0$, the detachment probability for positive helicity of the field is smaller than the one for the negative helicity, thus leading to the negative values of the elliptic-dichroism parameter. The situation is opposite for $p_y < 0$. These conclusions strongly depend on the value of the absolute phase φ_1. For an ultrashort driving pulse, the photoelectron momentum distribution can exhibit a smooth or an oscillatory behavior as a function of the photoelectron energy and the emission angle. For example, the momentum distribution shown in the left panel of Fig. 3 is oscillatory for $p_y > 0$, while it is relatively smooth in the region $p_y < 0$. Combining this with the fact that the change of the helicity of the driving field leads to the transformation $p_y \to -p_y$ implies the nonzero value of the elliptic-dichroism parameter. The region with an oscillatory differential detachment probability is determined by the value of the absolute phase φ_1. In particular, for $\varepsilon > 0$ and $\varphi_1 = 0^\circ$, the oscillatory character is most pronounced for the emission angle $\theta_e = 90^\circ$, while for an arbitrary value of the absolute phase φ_1, it is most pronounced for the emission angle $\theta_e = \varphi_1 + 90^\circ$. In other words, the region with oscillatory differential detachment probability rotates by the angle φ_1 in the counterclockwise direction. For the negative driving-field ellipticity, this rotation is in the clockwise direction. As a result, the elliptic-dichroism parameter is, on average, $\delta_{\mathbf{p}}(\varepsilon) < 0$ for $p_y > 0$ and $\delta_{\mathbf{p}}(\varepsilon) > 0$ for $p_y < 0$ for the absolute phase $\varphi_1 \in (-\pi/2, \pi/2)$, it is exactly zero for $\varphi_1 = \pm\pi/2$, and, on average, $\delta_{\mathbf{p}}(\varepsilon) > 0$ for $p_y > 0$ and $\delta_{\mathbf{p}}(\varepsilon) < 0$ for $p_y < 0$ for the absolute phase $\varphi_1 \in (\pi/2, 3\pi/2)$. An accurate measurement of the absolute phase is important for various experimental setups. Consequently, many methods of the measuring of this parameter have been developed. For example, the absolute phase can be determined by attosecond streaking [51,52] and by analyzing the velocity map images of ATI from noble gases [53]. Also, by combining the single-shot absolute phase tagging technique with

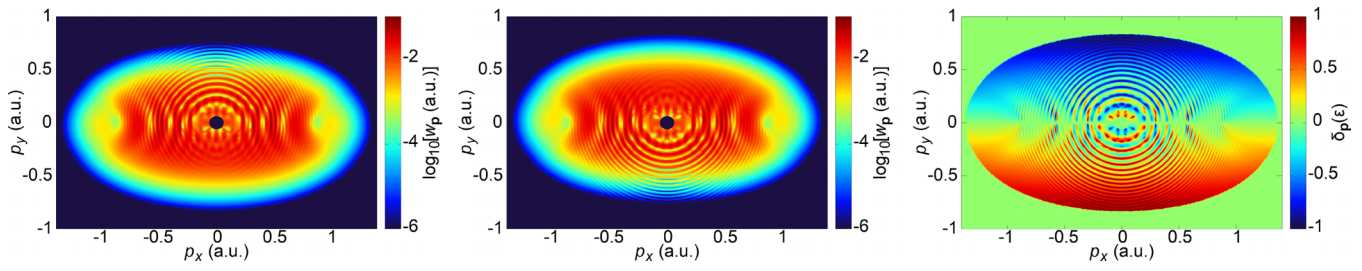

FIG. 3. Logarithm of the differential detachment probability of the direct electrons in the pulse polarization plane for the F^- ion exposed to the elliptically polarized field with ellipticity $\varepsilon = 0.2$ (left panel) and $\varepsilon = -0.2$ (middle panel), together with the corresponding elliptic-dichroism parameter (right panel). Other field parameters are the same as in Fig. 1.

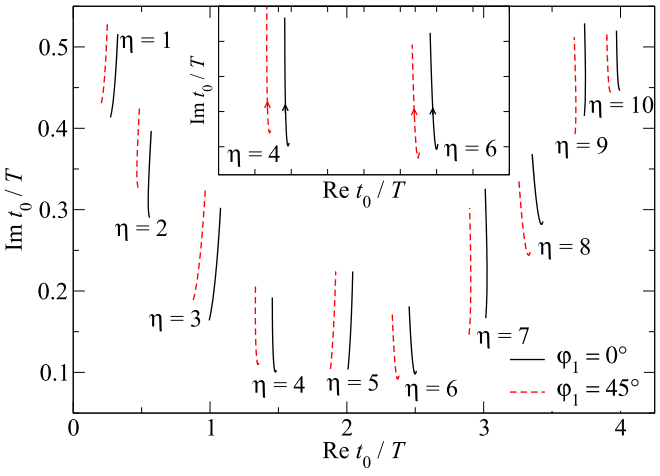

FIG. 4. Saddle-point solutions for the ATD electrons emitted in the direction $\theta_e = 70^\circ$, induced by the same laser field as in Fig. 1, for the absolute phases $\varphi_1 = 0^\circ$ (black solid lines) and $\varphi_1 = 45^\circ$ (red dashed lines). The inset shows the solutions which lead to the most significant contributions to the differential detachment probability.

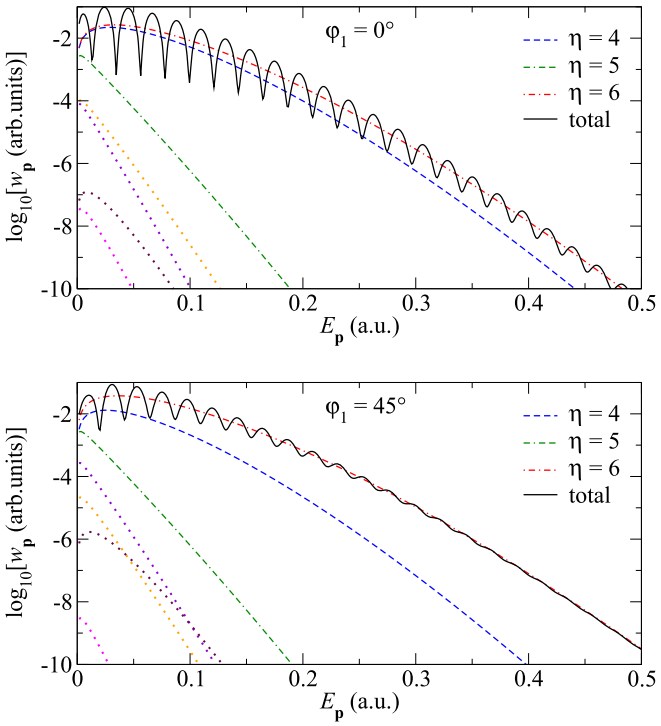

FIG. 5. Partial contributions to the differential detachment probability for the SP solutions from Fig. 4, together with the total differential detachment probability (black solid line). The dominant partial contributions of the SP solutions to the differential detachment probability are shown by the blue dashed, green double-dash-dotted, and red dash-dotted lines, while the contributions which can be neglected are denoted by the orange, maroon, violet, and magenta dotted lines.

cold-target recoil-ion momentum spectroscopy and velocity-map imaging, it is possible to investigate and control the absolute-phase-dependent processes with attosecond resolution [54]. The fact that the elliptic-dichroism parameter is zero only for a limited number of values of the absolute phase can be used as a method for measuring this phase. In particular, the zero value of the elliptic-dichroism parameter indicates that the absolute phase is $\varphi_1 = \pm\pi/2$.

The effect of the absolute phase on the photoelectron momentum distribution and the elliptic-dichroism parameter can also be investigated using the SP method. In Fig. 4 we present the solutions of the SP equation (5), i.e., the ionization time in the complex plane, for the F^- ion exposed to the same field as in Fig. 1 for two values of the absolute phase: $\varphi_1 = 0^\circ$ (black solid lines) and $\varphi_1 = 45^\circ$ (red dashed lines). The emission angle is $\theta_e = 70^\circ$, while the photoelectron energy changes from 0 a.u. to 0.83 a.u. along the curves. For an elliptically polarized ultrashort pulse, there are $2(n_p + 1)$ SP solutions in the upper half of the complex plane [55]. These solutions are denoted by the integer number η which increases with the increase of the real part of the ionization time. Keeping in mind that the increase of the imaginary part of the ionization time causes the exponential decrease of the differential detachment probability, we conclude that the solutions with dominant contributions are $\eta = 4$ and $\eta = 6$, while the solution $\eta = 5$ contributes significantly only in the low-energy region. In Fig. 5 we present the partial contributions to the differential detachment probability for the SP solutions from Fig. 4 for the absolute phase $\varphi_1 = 0^\circ$ (upper panel) and $\varphi_1 = 45^\circ$ (lower panel). The solutions $\eta = 4$ and $\eta = 6$ dominantly determine the spectra in both cases. However, for the absolute phase $\varphi_1 = 0^\circ$ these two contributions are comparable, which causes rapid oscillations of the differential detachment probability as a function of the photoelectron energy. In other words, these two contributions interfere and, depending on the photoelectron energy, this interference can be either constructive or destructive. On the other hand, for the absolute phase $\varphi_1 = 45^\circ$ the contribution of the solution $\eta = 6$ is more significant than the contribution of the solution $\eta = 4$, so that the oscillations due to the interference of these contributions are less pronounced. Consequently, the spectrum is much more smooth than for the absolute phase $\varphi_1 = 0^\circ$. This behavior can be understood if we look back to the complex solutions for the ionization time. In particular, the inset of Fig. 4 shows the solutions $\eta = 4$ and $\eta = 6$ for both values of the absolute phase φ_1. The change of the absolute phase from $\varphi_1 = 0^\circ$ to $\varphi_1 = 45^\circ$ slightly increases (decreases) the imaginary part of the ionization time for the solution $\eta = 4$ ($\eta = 6$). As a result, the difference between the partial contributions with $\eta = 4$ and $\eta = 6$ is more pronounced for the value of the absolute phase $\varphi_1 = 45^\circ$ than for $\varphi_1 = 0^\circ$. An analogous analysis can be done for other values of the absolute phase and the emission angle. In conclusion, although the direct electrons spend only a short time under the influence of the driving field, the change of the absolute phase can still significantly alter the differential detachment probability thus changing the response of the system to the change of the helicity of the driving field.

Finally, we investigate how the ellipticity of the driving field affects the elliptic-dichroism parameter. As the ellipticity of the driving field increases, the imaginary part of the ionization time for the solutions $\eta = 1, 3, 5, 7, 9$ also increases, thus leading to an exponential decrease of the differential

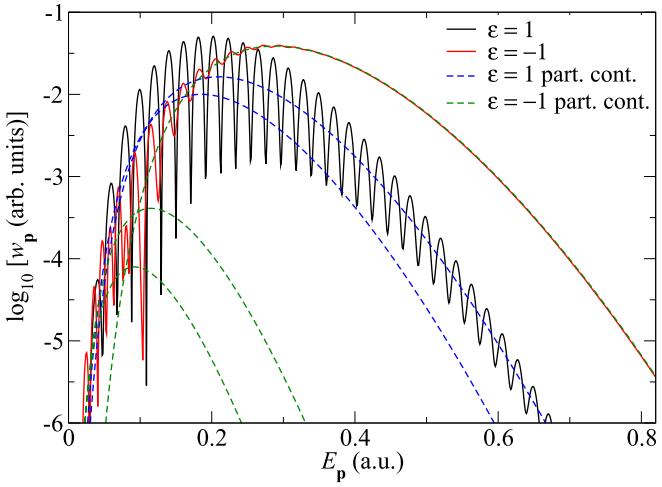

FIG. 6. Logarithm of the differential detachment probability for the F^- ion exposed to the circularly polarized field with $\varepsilon = 1$ (black solid line) and $\varepsilon = -1$ (red solid line), together with the partial contributions of different SP solutions (dashed lines). The emission angle is $\theta_e = 70^\circ$ and the absolute phase is $\varphi_1 = 0^\circ$, while other field parameters are the same as in Fig. 1.

detachment probability. Specifically, for the ellipticity larger than some critical value the number of SP solutions is effectively halved. In the limit of a circularly polarized driving pulse, there are only $n_p + 1$ (in our case five) solutions of the SP equation [55]. For the absolute phase $\varphi_1 = 0^\circ$ and the ellipticity $\varepsilon > 0.2$, the conclusions about the elliptic-dichroism parameter are similar to those related to the results shown in Fig. 3. However, for a large driving-field ellipticity ($\varepsilon > 0.55$) and $p_y > 0$, the elliptic-dichroism parameter is positive in the low-energy region of the spectrum for a wide range of the values of the emission angle θ_e. This behavior becomes more pronounced as we approach to a circularly polarized field. In Fig. 6 we compare the photoelectron energy spectra obtained using the circularly polarized field with $\varepsilon = 1$ (black solid line) and $\varepsilon = -1$ (red solid line). The corresponding SP partial contributions are presented by the blue dashed and green dashed lines, respectively. For the driving-field ellipticity $\varepsilon = 1$, the spectrum is determined by two SP solutions, while for the case with $\varepsilon = -1$, the spectrum is determined by only one SP solution for $E_\mathbf{p} > 0.15$ a.u., while the other two solutions also contribute significantly for $E_\mathbf{p} < 0.15$ a.u. Clearly, for $E_\mathbf{p} < 0.25$ a.u., the differential detachment probability is higher for $\varepsilon = 1$ than for $\varepsilon = -1$ for most values of the photoelectron energy, thus leading to the overall positive elliptic-dichroism parameter. Still, due to the oscillatory character of both spectra, this is not true for all but for most values of the photoelectron energy $E_\mathbf{p} < 0.25$ a.u. On the other hand, for $E_\mathbf{p} > 0.25$ a.u. the differential detachment probability is higher for $\varepsilon = -1$ than for $\varepsilon = 1$ (these conclusions are the same as for the driving field with $\varepsilon = \pm 0.2$).

B. Bi-elliptical field

After analyzing the elliptically polarized driving field, we now turn our attention to the more complex case of a bi-elliptical field, i.e., to the field $\mathbf{E}(t) = \mathbf{E}_1(t) + \mathbf{E}_2(t)$, with the components given by Eqs. (8). This field becomes an orthogonally polarized two-color (OTC) field for $\varepsilon_1 = \varepsilon_2 = 0$, while the case $\varepsilon_1 = \varepsilon_2 = 1$ corresponds to a counterrotating bicircular field [56]. As an example, we consider the F^- ion exposed to the ω–2ω bi-elliptical field with the component intensity $I = E_1^2 = E_2^2 = 8 \times 10^{12}$ W/cm^2, fundamental wavelength of 2000 nm, absolute phases $\varphi_1 = 0^\circ$ and $\varphi_2 = 90^\circ$, and equal ellipticity $\varepsilon = \varepsilon_1 = \varepsilon_2$ of both components.

In Fig. 7 we present the logarithm of the differential detachment probability of the F^- ion in the ω–2ω bi-elliptical field with the ellipticities $\varepsilon = 0.4$ (left panel) and $\varepsilon = -0.4$ (middle panel), together with the corresponding elliptic-dichroism parameter (right panel). A careful comparison of the spectra obtained for $\varepsilon = \pm 0.4$ reveals quantitative differences. For example, for the emission angle around $\theta_e = 90^\circ$ the spectrum obtained with $\varepsilon = -0.4$ is slightly longer than the spectrum obtained with $\varepsilon = 0.4$. Similar conclusions hold for the emission in the direction around $\theta_e = -45^\circ$. Contrary to the case of an elliptically polarized field, the spectra obtained by a bi-elliptical field with $\varepsilon = \pm 0.4$ are not related by any reflection symmetry. The difference between these spectra is quantified by the elliptic-dichroism parameter (see the right panel of Fig. 7). This parameter reveals that the most pronounced difference between the two spectra appears near the cutoff for the emission angle $45^\circ < \theta_e < 180^\circ$, where the differential detachment probability is much larger for $\varepsilon = -0.4$. Besides this region, there are many other regions with the elliptic-dichroism parameter close to ± 1.

At this place, it is illustrative to compare the symmetry properties of our photoelectron momentum distributions with those of the distributions obtained using a long pulse with a flat envelope. As we mentioned in Sec. III A, the symmetry properties inherent to the HATD spectra are related to the symmetry properties of the driving field. For a long pulse with a flat envelope, the transformation $t \to t + T/2$ changes the electric field (8) as $\mathbf{E}_1(t + T/2) = (-1)^r \mathbf{E}_1(t)$ and $\mathbf{E}_2(t + T/2) = (-1)^s \mathbf{E}_2(t)$ with the similar transformation law for the vector potential [49,50]. More precisely, our field $\mathbf{E}(t)$ becomes the field employed in [49] when $f(t) = 1$ and $\varphi_1 = \varphi_2 = -\pi/2$. In this case, for both the ATD and HATD electrons, the change of the sign of the component ellipticities leads to the reflection with respect to the p_y axis, i.e., the photoelectron momentum distribution obtained using the field with the component ellipticities $\varepsilon_1, \varepsilon_2$ is a mirror image of the photoelectron momentum distribution obtained with the ellipticities $-\varepsilon_1, -\varepsilon_2$ (see Figs. 2 and 8 in [49]). The situation is different for the few-cycle pulse elaborated in the present paper. In particular, the change of the sign of the component ellipticities does not lead to a simple transformation of the applied field. For a few-cycle bi-elliptical driving pulse the photoelectron momentum distribution is changed quantitatively by changing the sign of the component ellipticities (cf. the left and middle panels of Fig. 7). In conclusion, for an ultrashort driving pulse, the nonzero elliptic-dichroism parameter is a consequence of the lack of the rotational and reflection symmetries of the driving pulse and the corresponding vector potential. In addition, the shape of the momentum distribution depends on the values of the absolute phases.

A particularly interesting example is a bicircular field employed as a driving field. In Fig. 8 we display the

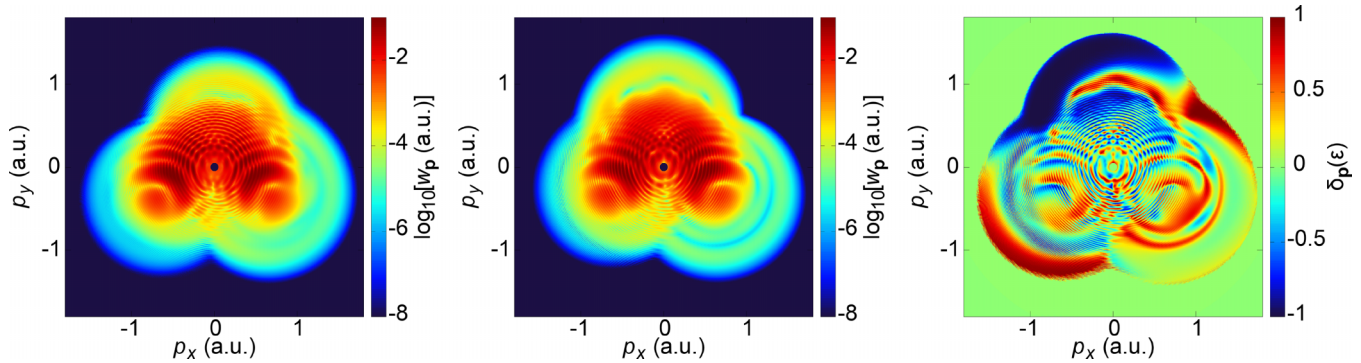

FIG. 7. Logarithm of the differential detachment probability in the pulse polarization plane for the F^- ion exposed to the ω–2ω bi-elliptical field with the ellipticity $\varepsilon = 0.4$ (left panel) and $\varepsilon = -0.4$ (middle panel), together with the corresponding elliptic-dichroism parameter (right panel). The intensity of both field components is $I = E_1^2 = E_2^2 = 8 \times 10^{12}$ W/cm^2, while the fundamental wavelength is 2000 nm and the absolute phases are $\varphi_1 = 0^\circ$ and $\varphi_2 = 90^\circ$.

photoelectron momentum distribution for the F^- ion ionized by the ω–2ω bicircular field with the same parameters as in Fig. 7. A three-lobe structure typical for this field is clearly visible. However, contrary to the situation in which a long pulse with a flat envelope is used as a driving field, our spectrum does not obey the rotational symmetry with respect to the rotation by the angle $2\pi j/3$ with integer j. This can easily be confirmed by a careful comparison of the lobes in Fig. 8. For example, the position of the cutoff is the lowest for the lobe centered around the direction $\theta_e = 90^\circ$, while it is the highest for the lobe centered around $\theta_e = -30^\circ$. Furthermore, in the first case, the differential detachment probability has an oscillatory character as a function of the photoelectron energy, while in the second case the oscillations of the differential detachment probability as a function of the photoelectron energy are less pronounced. Additionally, the quantitative difference of the differential detachment probability for different lobes, as well as the position of the cutoff, depend on the values of the absolute phases φ_1 and φ_2. Moreover, the change of the absolute phase φ_2 with the fixed phase φ_1 leads to the rotation of the lobes by the angle $-\varphi_2/3$, simultaneously changing the differential detachment probability and the length of the rescattering plateau. As the length of the pulse increases, the difference of the differential detachment probability and the position of the cutoff for the three above-mentioned lobes become less pronounced. Finally, it is important to stress that the quantitative discussions about the elliptic-dichroism parameter are derived for fixed values of the absolute phases φ_1 and φ_2.

Similarly as in the case of an elliptically polarized field, the ATD electrons deserve particular attention. In Fig. 9 we present the results for direct detachment of electrons from the

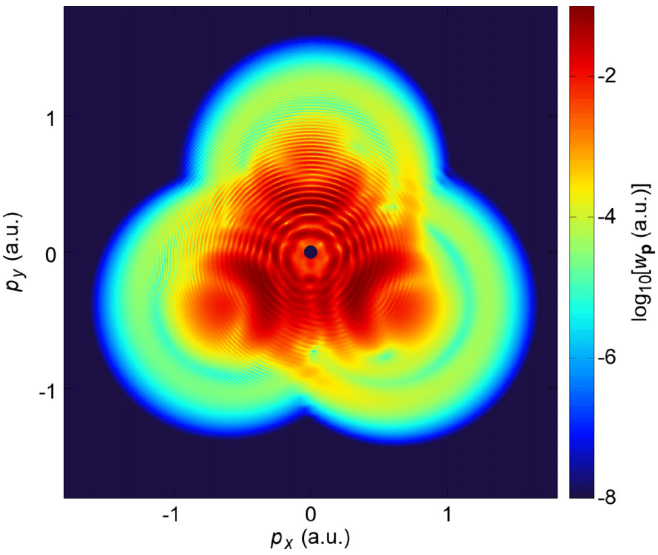

FIG. 8. Logarithm of the differential detachment probability in the pulse polarization plane for the F^- ion exposed to the bicircular field ($\varepsilon_1 = \varepsilon_2 = 1$) with other parameters the same as in Fig. 7. Both the direct and rescattered electrons are taken into consideration.

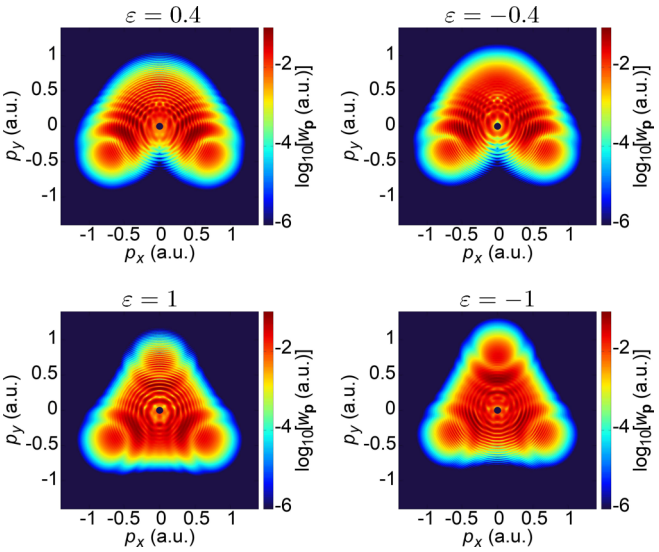

FIG. 9. Logarithm of the differential detachment probability of the direct electrons in the pulse polarization plane for the F^- ion exposed to the ω–2ω bi-elliptical field with the component intensity $I = E_1^2 = E_2^2 = 8 \times 10^{12}$ W/cm^2, fundamental wavelength of 2000 nm, and absolute phases $\varphi_1 = 0^\circ$ and $\varphi_2 = 90^\circ$. The ellipticity of the field components is the same and is indicated above the panels.

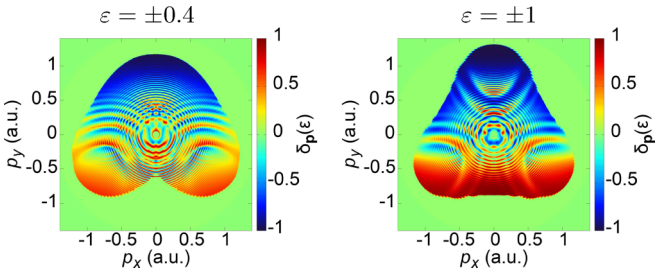

FIG. 10. Elliptic-dichroism parameter which corresponds to the spectra shown in Fig. 9. The ellipticity of the field components is the same and is indicated above the panels.

F^- ion by an ω–2ω bi-elliptical pulse. As we noticed while analyzing the elliptically polarized field, the ATD momentum distribution is closely related to the symmetry properties of the vector potential [Eq. (9)]. In particular, for the chosen values of the absolute phases, the time inversion $t \to -t$ transforms the vector potential as $A_x \to -A_x$ and $A_y \to A_y$. As a result, the spectra are invariant with respect to the reflection $p_x \to -p_x$ regardless of the ellipticity of the driving-field components. This reflection symmetry is clearly visible in all panels of Fig. 9. Moreover, it is the only reflection symmetry satisfied by the photoelectron momentum distributions, even for the case of a bicircular field. In more detail, contrary to the case of a long driving pulse with a flat envelope, the photoelectron momentum distribution obtained by a bicircular few-cycle pulse does not possess the reflection symmetry about the axes at the angles of 30° and 150° with respect to the positive p_x direction (cf. the lower panels of Fig. 9). Furthermore, the change of the helicity of the applied field does not lead to a simple transformation of the vector potential and the differential detachment probability is altered quantitatively by this transformation, thus leading to a nonzero elliptic-dichroism parameter. To illustrate this effect, in Fig. 10 we display the elliptic-dichroism parameter which corresponds to the spectra shown in Fig. 9 for the field ellipticity as indicated above the panels. On average, this parameter is negative for $p_y > 0$ and positive for $p_y < 0$. This effect becomes more pronounced with the increase of the driving-field ellipticity. Finally, it is important to mention that the reflection symmetry $p_x \to -p_x$, obeyed by the spectra and elliptic-dichroism parameter shown in Figs. 9 and 10 is broken when the rescattered electrons are taken into consideration. This also holds for the low-energy region due to the interference of the direct and rescattered amplitudes (see the low-energy region in the right panel of Fig. 7). A typical experiment does not distinguish between the direct and rescattered electrons so that the reflection symmetry can be considered as an approximate symmetry of the photoelectron momentum distribution due to the fact that the rescattered electrons have a much lower differential detachment probability.

The influence of the helicity switch can also be examined using the SP method. In Fig. 11 we present the solutions of the SP equation (5) (bottom panels) which contribute significantly to the ATD spectrum obtained by exposing the F^- ion to the ω–2ω bi-elliptical field with the component ellipticity $\varepsilon = 0.4$ (left column) and $\varepsilon = -0.4$ (right column) for the emission angle $\theta_e = 45°$. The photoelectron energy changes from 0 a.u. to 0.83 a.u. along the curves. In addition, the parameter $E = \sqrt{E_1^2 + E_2^2}$ is shown in the top panels of Fig. 11. Equation (5) has $(n_p + 1)(r + s) = 15$ solutions for this field configuration. This can easily be derived following the procedure given in [55,57]. The solutions which lead to the most significant contributions to the differential detachment probability are $\eta = 6, 7, 8, 9$ for $\varepsilon = 0.4$ and $\eta = 6, 7, 9, 10$ for $\varepsilon = -0.4$. Comparing the top and bottom panels of Fig. 11 it is evident that the real parts of the ionization time for these solutions are close to the center of the pulse and, for these values of the ionization time, the parameter $E = \sqrt{E_1^2 + E_2^2}$ is maximal. The partial contributions of these SP solutions are shown in Fig. 12 (dashed, dotted, dash-dotted, double dash-dotted lines) together with the total spectra (black solid line) for $\varepsilon = 0.4$ (upper panel) and $\varepsilon = -0.4$ (lower panel). In both cases the dominant contribution comes from the solution $\eta = 9$ (blue dashed lines in Fig. 12), while other solutions

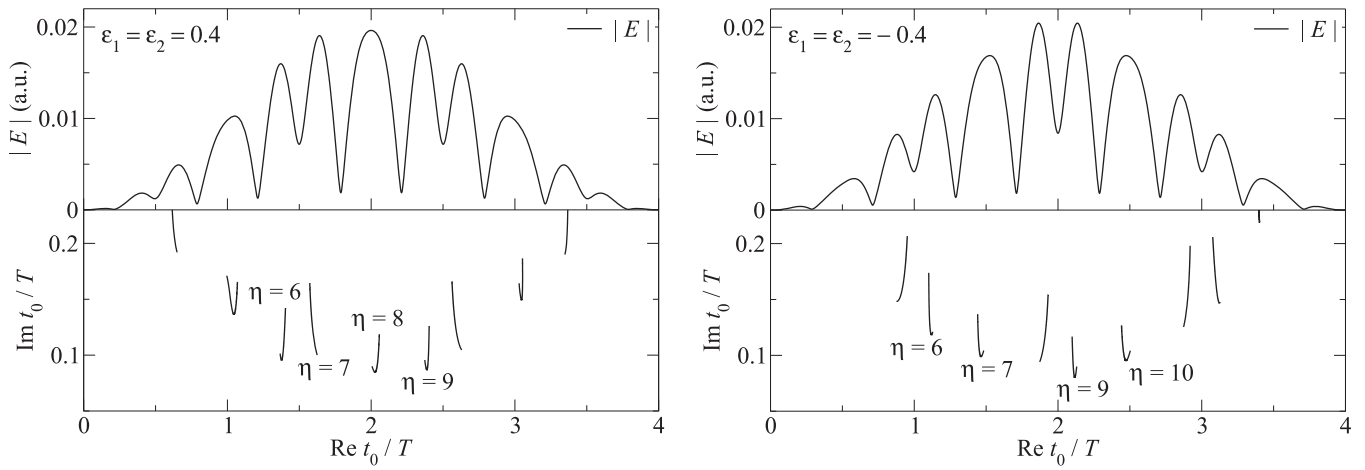

FIG. 11. Upper row: Parameter $E = \sqrt{E_1^2 + E_2^2}$ for the ω–2ω bi-elliptical field as a function of the time for the ellipticity as indicated in the panels. Lower row: Saddle-point solutions for the ATD electrons emitted in the direction $\theta_e = 45°$. The photoelectron energy changes from 0 a.u. to 0.83 a.u. along the curves. Left (right) panels: $\varepsilon_1 = \varepsilon_2 = 0.4$ ($\varepsilon_1 = \varepsilon_2 = -0.4$). Field parameters are the same as in Fig. 7.

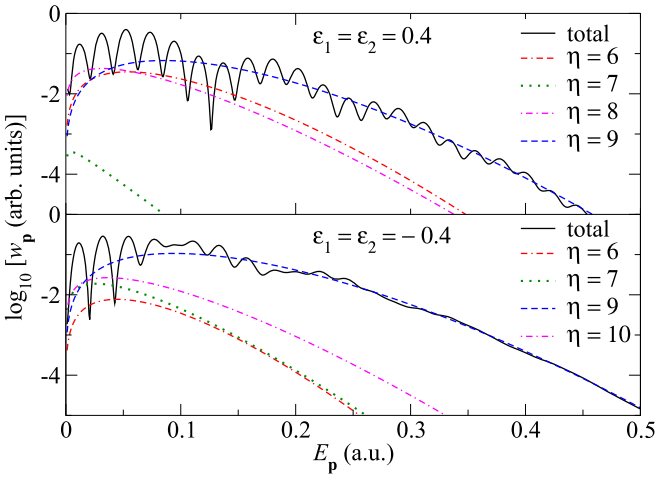

FIG. 12. Logarithm of the differential detachment probability for the F^- ion exposed to the ω–2ω bi-elliptical field with $\varepsilon_1 = \varepsilon_2 = 0.4$ (upper panel) and $\varepsilon_1 = \varepsilon_2 = -0.4$ (lower panel), together with the partial contributions of the SP solutions as indicated in the legends. The emission angle is $\theta_e = 45°$, while the field parameters are the same as in Fig. 7.

can eventually become significant in the low-energy part of the spectrum. The main reason why the elliptic-dichroism parameter is negative for this direction can be explained by analyzing the behavior of the solution $\eta = 9$, particularly in the medium- and high-energy part of the spectrum. Comparing the lower-row panels in Fig. 11 we see that the imaginary part of the ionization time is generally smaller for $\varepsilon = -0.4$ than for $\varepsilon = 0.4$. This can be related to the value of the parameter $E = \sqrt{E_1^2 + E_2^2}$. For example, for the photoelectron energy $E_{\mathbf{p}} = 0.2$ a.u. we have $\mathrm{Re}\, t_0 = 2.397T$ and $E = 1.758 \times 10^{-2}$ a.u. for $\varepsilon = 0.4$, while for $\varepsilon = -0.4$ it is $\mathrm{Re}\, t_0 = 2.107T$ and $E = 1.955 \times 10^{-2}$ a.u. This means that, in the later case, the electron is exposed to the stronger field during and after the ionization process which leads to the lower imaginary part of the ionization time $\mathrm{Im}\, t_0$ and consequently larger differential detachment probability. This explains the negative value of the elliptic-dichroism parameter (see the left panel of Fig. 10). One should keep in mind that the differential detachment probability exponentially decreases with the increase of the imaginary part of the ionization time so that a small decrease of $\mathrm{Im}\, t_0$ can significantly change the differential detachment probability. Finally, we mention that some other solutions of the SP equation are also affected by the change of the helicity of the driving field, but still they only affect the low-energy part of the spectrum.

IV. CONCLUSION

In recent years, laser pulses with a duration of only few optical cycles have become readily available in the mid-IR region [58]. These led to the discovery of many new effects, the examples of which were discussed in [59–61]. Particularly interesting are the laser fields which evolve in the plane, thus leading to a rich two-dimensional electron dynamics. These fields include the elliptically polarized field and bi-elliptical fields. In both cases, there are many parameters which can be used as control knobs. Especially interesting parameters are the ellipticity of the field components and the absolute phase. In particular, the photoelectron momentum distribution in the laser-field polarization plane significantly depends on the helicity of the applied-field components. This effect is called the elliptic dichroism in the photoelectron momentum distribution and it represents an important tool for the investigation of the interaction of an electromagnetic field with matter [62]. The elliptic dichroism can be successfully quantified using the elliptic-dichroism parameter which represents the normalized difference between the photoelectron yields calculated for the driving fields with opposite helicity. The photoelectron momentum distribution can also be successfully controlled using the absolute phase of the applied field as a control parameter. This particularly holds for the regions of the pulse polarization plane where the rescattered electrons are dominant.

In this paper, we investigated the detachment of the electron from the negative fluorine ion exposed to strong elliptical or bi-elliptical few-cycle driving pulses in the framework of the strong-field approximation. After the ionization, the residual system is a neutral atom so that the SFA should be particularly successful due to the lack of the Coulomb effects. First, we explored the symmetry properties of the obtained momentum distributions. For an elliptically polarized few-cycle driving pulse, the photoelectron momentum distribution does not exhibit rotational and reflection symmetries. This is because of the absence of these symmetries for the applied electric field vector and the corresponding vector potential. The change of the helicity of the driving pulse leads to the reflection $p_y \to -p_y$, which is not a symmetry transformation of the photoelectron momentum distribution, so that the elliptic dichroism is well pronounced. This holds for both the direct and the rescattered electrons, i.e., even the direct electrons are sensitive to the helicity of the applied field, which was not the case for a long driving pulse with a flat envelope. In the region where the direct electrons are dominant, the elliptic-dichroism parameter is a relatively smooth function of the photoelectron energy and emission angle, while in the rescattering region it exhibits rapid oscillations as a function of the photoelectron energy. Moreover, for the direct electrons, the elliptic dichroism is zero only for a limited number of values of the absolute phase ($\varphi_1 = \pm\pi/2$). Therefore, the measurement of the elliptic dichroism can be used to accurately determine the value of this phase, i.e., if the elliptic-dichroism parameter is zero, the absolute phase is $\pm\pi/2$. Using the saddle-point method, we explained the nonzero value of the elliptic-dichroism parameter for the direct electrons, as well as the dependence of the photoelectron momentum distribution on the absolute phase. Finally, in order for the rescattered electrons to have a nonnegligible differential detachment probability, the ellipticity of the driving field should be small ($\varepsilon < 0.4$).

We also analyzed the detachment of electrons from negative ions exposed to a bi-elliptical driving field. We illustrated our findings using the example of a fluorine negative ion exposed to an ω–2ω bi-elliptical field with the component ellipticity $\varepsilon = 0.4$. The spectra obtained using the fields with opposite helicity are not related by any reflection symmetry and the elliptic-dichroism parameter does not exhibit any

particular rotational or reflection symmetry. We also discussed how the absolute phase affects the photoelectron momentum distribution. For the ω–2ω few-cycle bicircular field, the three lobes which appear in the momentum distribution are not the same either qualitatively or quantitatively. The length of the rescattering plateau, as well as the differential detachment probability itself, depend on the absolute phase. The change of this parameter does not simply lead to the rotation of the spectra as is the case for a long driving pulse with a flat envelope, but also changes the photoelectron yield quantitatively. In the end, we investigated the effects of the helicity switch on the direct photoelectron momentum distribution by employing the saddle-point method. In particular, using the saddle-point solutions which contribute significantly to the differential detachment probability, we accurately reproduced the spectra for the opposite field helicity, thus explaining the behavior of the elliptic-dichroism parameter as a function of the photoelectron energy and emission angle.

ACKNOWLEDGMENTS

We gratefully acknowledge support by the Ministry for Science, Higher Education, and Youth, Canton Sarajevo, Bosnia and Herzegovina.

[1] W. Becker, F. Grasbon, R. Kopold, D. B. Milošević, G. G. Paulus, and H. Walther, Above-threshold ionization: From classical features to quantum effects, Adv. At. Mol. Opt. Phys. **48**, 35 (2002).

[2] D. B. Milošević and F. Ehlotzky, Scattering and reaction processes in powerful laser fields, Adv. At. Mol. Opt. Phys. **49**, 373 (2003).

[3] D. B. Milošević, G. G. Paulus, D. Bauer, and W. Becker, Above-threshold ionization by few-cycle pulses, J. Phys. B: At. Mol. Opt. Phys. **39**, R203 (2006).

[4] M. C. Kohler, T. Pfeifer, K. Z. Hatsagortsyan, and C. H. Keitel, Frontiers of atomic high-harmonic generation, Adv. At. Mol. Opt. Phys. **61**, 159 (2012).

[5] P. Agostini and L. F. DiMauro, Atomic and molecular ionization dynamics in strong laser fields: From optical to x-rays, Adv. At. Mol. Opt. Phys. **61**, 117 (2012).

[6] S. V. Popruzhenko, Keldysh theory of strong field ionization: History, applications, difficulties and perspectives, J. Phys. B: At. Mol. Opt. Phys. **47**, 204001 (2014).

[7] F. Calegari, G. Sansone, S. Stagira, C. Vozzi, and M. Nisoli, Advances in attosecond science, J. Phys. B: At. Mol. Opt. Phys. **49**, 062001 (2016).

[8] W. Becker, S. P. Goreslavski, D. B. Milošević, and G. G. Paulus, The plateau in above-threshold ionization: The keystone of rescattering physics, J. Phys. B: At. Mol. Opt. Phys. **51**, 162002 (2018).

[9] K. Amini, J. Biegert, F. Calegari, A. Chacón, M. F. Ciappina, A. Dauphin, D. K. Efimov, C. Figueira de Morisson Faria, K. Giergiel, P. Gniewek, A. S. Landsman, M. Lesiuk, M. Mandrysz, A. S. Maxwell, R. Moszyński, L. Ortmann, J. A. Pérez-Hernández, A. Picón, E. Pisanty, J. Prauzner-Bechcicki *et al.*, Symphony on strong field approximation, Rep. Prog. Phys. **82**, 116001 (2019).

[10] M. Nisoli, S. De Silvestri, O. Svelto, R. Szipöcs, K. Ferencz, Ch. Spielmann, S. Sartania, and F. Krausz, Compression of high-energy laser pulses below 5 fs, Opt. Lett. **22**, 522 (1997).

[11] M. Hemmer, M. Baudisch, A. Thai, A. Couairon, and J. Biegert, Self-compression to sub-3-cycle duration of mid-infrared optical pulses in dielectrics, Opt. Express **21**, 28095 (2013).

[12] F. Krausz and M. Ivanov, Attosecond physics, Rev. Mod. Phys. **81**, 163 (2009).

[13] M. Drescher, M. Hentschel, R. Kienberger, G. Tempea, C. Spielmann, G. A. Reider, P. B. Corkum, and F. Krausz, X-ray pulses approaching the attosecond frontier, Science **291**, 1923 (2001).

[14] K. Zhao, Q. Zhang, M. Chini, Y. Wu, X. Wang, and Z. Chang, Tailoring a 67 attosecond pulse through advantageous phase-mismatch, Opt. Lett. **37**, 3891 (2012).

[15] F. Silva, S. M. Teichmann, S. L. Cousin, M. Hemmer, and J. Biegert, Spatio-temporal isolation of attosecond soft x-ray pulses in the water window, Nat. Commun. **6**, 6611 (2015).

[16] D. Habibović, W. Becker, and D. B. Milošević, Attosecond pulse trains with elliptical polarization from an orthogonally polarized two-color field, J. Opt. Soc. Am. B **38**, 3367 (2021).

[17] J. Itatani, J. Levesque, D. Zeidler, H. Niikura, H. Pépin, J. C. Kieffer, P. B. Corkum, and D. M. Villeneuve, Tomographic imaging of molecular orbitals, Nature (London) **432**, 867 (2004).

[18] C. I. Blaga, J. Xu, A. D. DiChiara, E. Sistrunk, K. Zhang, P. Agostini, T. A. Miller, L. F. DiMauro, and C. D. Lin, Imaging ultrafast molecular dynamics with laser-induced electron diffraction, Nature (London) **483**, 194 (2012).

[19] L. Nahon, L. Nag, G. A. Garcia, I. Myrgorodska, U. Meierhenrich, S. Beaulieu, V. Wanie, V. Blanchet, R. Géneaux, and I. Powis, Determination of accurate electron chiral asymmetries in fenchone and camphor in the VUV range: Sensitivity to isomerism and enantiomeric purity, Phys. Chem. Chem. Phys. **18**, 12696 (2016).

[20] A. de Bohan, P. Antoine, D. B. Milošević, and B. Piraux, Phase-Dependent Harmonic Emission with Ultrashort Laser Pulses, Phys. Rev. Lett. **81**, 1837 (1998).

[21] G. G. Paulus, F. Grasbon, H. Walther, P. Villoresi, M. Nisoli, S. Stagira, E. Priori, and S. Silvestri, Absolute-phase phenomena in photoionization with few-cycle laser pulses, Nature (London) **414**, 182 (2001).

[22] D. B. Milošević, G. G. Paulus, and W. Becker, Phase-Dependent Effects of a Few-Cycle Laser Pulse, Phys. Rev. Lett. **89**, 153001 (2002).

[23] D. B. Milošević, G. G. Paulus, and W. Becker, High-order above-threshold ionization with few-cycle pulse: A meter of the absolute phase, Opt. Express **11**, 1418 (2003).

[24] G. G. Paulus, F. Lindner, H. Walther, A. Baltuška, E. Goulielmakis, M. Lezius, and F. Krausz, Measurement of the Phase of Few-Cycle Laser Pulses, Phys. Rev. Lett. **91**, 253004 (2003).

[25] A. Baltuška, T. Udem, M. Uiberacker, M. Hentschel, E. Goulielmakis, Ch. Gohle, R. Holzwarth, V. S. Yakovlev,

A. Scrinzi, T. W. Hänsch, and F. Krausz, Attosecond control of electronic processes by intense light fields, Nature (London) **421**, 611 (2003).

[26] J. M. Ngoko Djiokap, S. X. Hu, L. B. Madsen, N. L. Manakov, A. V. Meremianin, and A. F. Starace, Electron Vortices in Photoionization by Circularly Polarized Attosecond Pulses, Phys. Rev. Lett. **115**, 113004 (2015).

[27] J. M. N. Djiokap, A. V. Meremianin, N. L. Manakov, S. X. Hu, L. B. Madsen, and A. F. Starace, Kinematical vortices in double photoionization of helium by attosecond pulses, Phys. Rev. A **96**, 013405 (2017).

[28] K.-J. Yuan, S. Chelkowski, and A. D. Bandrauk, Photoelectron momentum distributions of molecules in bichromatic circularly polarized attosecond UV laser fields, Phys. Rev. A **93**, 053425 (2016).

[29] K.-J. Yuan, H. Lu, and A. D. Bandrauk, Photoionization of triatomic molecular ions H_3^{2+} by intense bichromatic circularly polarized attosecond UV laser pulses, J. Phys. B: At. Mol. Opt. Phys. **50**, 124004 (2017).

[30] D. Pengel, S. Kerbstadt, D. Johannmeyer, L. Englert, T. Bayer, and M. Wollenhaupt, Electron Vortices in Femtosecond Multiphoton Ionization, Phys. Rev. Lett. **118**, 053003 (2017).

[31] G. S. J. Armstrong, D. D. A. Clarke, J. Benda, J. Wragg, A. C. Brown, and H. W. van der Hart, Modeling tomographic measurements of photoelectron vortices in counter-rotating circularly polarized laser pulses, Phys. Rev. A **100**, 063416 (2019).

[32] L. Geng, F. Cajiao Vélez, J. Z. Kamiński, L.-Y. Peng, and K. Krajewska, Vortex structures in photodetachment by few-cycle circularly polarized pulses, Phys. Rev. A **102**, 043117 (2020).

[33] M. M. Majczak, F. Cajiao Vélez, J. Z. Kamiński, and K. Krajewska, Carrier-envelope-phase and helicity control of electron vortices and spirals in photodetachment, Opt. Express **30**, 43330 (2022).

[34] W.-Y. Wu and F. He, Asymmetric photoelectron momentum distribution driven by two-color XUV fields, Phys. Rev. A **93**, 023415 (2016).

[35] K.-J. Yuan and A. D. Bandrauk, Above-threshold ionization in molecules by intense multiple-frequency circularly polarized laser pulses, Phys. Rev. A **98**, 023413 (2018).

[36] S. Eckart, D. Trabert, K. Fehre, A. Geyer, J. Rist, K. Lin, F. Trinter, L. P. H. Schmidt, M. S. Schöffler, T. Jahnke, M. Kunitski, and R. Dörner, Sideband modulation by subcycle interference, Phys. Rev. A **102**, 043115 (2020).

[37] A. V. Flegel, N. L. Manakov, A. V. Sviridov, M. V. Frolov, L. Geng, and L.-Y. Peng, Analytic description of the above-threshold detachment in the adiabatic limit, Phys. Rev. A **102**, 063119 (2020).

[38] J. Hofbrucker, B. Böning, A. V. Volotka, and S. Fritzsche, Elliptical dichroism in biharmonic ionization of atoms, Phys. Rev. A **104**, 013102 (2021).

[39] D. Peng, L.-W. Pi, M. V. Frolov, and A. F. Starace, Enhancing high-order-harmonic generation by time delays between two-color, few-cycle pulses, Phys. Rev. A **95**, 033413 (2017).

[40] M. V. Frolov, N. L. Manakov, A. A. Minina, N. V. Vvedenskii, A. A. Silaev, M. Y. Ivanov, and A. F. Starace, Control of Harmonic Generation by the Time Delay Between Two-Color, Bicircular Few-Cycle Mid-IR Laser Pulses, Phys. Rev. Lett. **120**, 263203 (2018).

[41] A. Gazibegović-Busuladžić, D. B. Milošević, W. Becker, B. Bergues, H. Hultgren, and I. Y. Kiyan, Electron Rescattering in Above-Threshold Photodetachment of Negative Ions, Phys. Rev. Lett. **104**, 103004 (2010).

[42] A. Kramo, E. Hasović, D. B. Milošević, and W. Becker, Above-threshold detachment by a two-color bicircular laser field, Laser Phys. Lett. **4**, 279 (2007).

[43] A. Gazibegović-Busuladžić, D. Habibović, M. Busuladžić, and D. B. Milošević, Molecular strong-field approximation for photodetachment of electrons from homonuclear diatomic molecular anions, J. Opt. Soc. Am. B **37**, 813 (2020).

[44] B. Fetić, D. B. Milošević, and W. Becker, High-order above-threshold ionisation of atoms and negative ions: Channel-closing effects and the low-frequency approximation, J. Mod. Opt. **58**, 1149 (2011).

[45] A. A. Radzig and B. M. Smirnov, *Reference Data on Atoms, Molecules, and Ions* (Springer, Berlin, 1985).

[46] X. X. Zhou, Z. Chen, T. Morishita, A.-T. Le, and C. D. Lin, Retrieval of electron-atom scattering cross sections from laser-induced electron rescattering of atomic negative ions in intense laser fields, Phys. Rev. A **77**, 053410 (2008).

[47] G. F. Gribakin and M. Y. Kuchiev, Multiphoton detachment of electrons from negative ions, Phys. Rev. A **55**, 3760 (1997).

[48] A. Gazibegović-Busuladžić, D. B. Milošević, and W. Becker, High-energy above-threshold detachment from negative ions, Phys. Rev. A **70**, 053403 (2004).

[49] W. Becker and D. B. Milošević, Elliptic dichroism in strong-field ionization of atoms subjected to tailored laser fields, Phys. Chem. Chem. Phys. **24**, 7014 (2022).

[50] D. Habibović, W. Becker, and D. B. Milošević, Symmetries and selection rules of the spectra of photoelectrons and high-order harmonics generated by field-driven atoms and molecules, Symmetry **13**, 1566 (2021).

[51] R. Kienberger, E. Goulielmakis, M. Uiberacker, A. Baltuska, V. Yakovlev, F. Bammer, A. Scrinzi, T. Westerwalbesloh, U. Kleineberg, U. Heinzmann, M. Drescher, and F. Krausz, Atomic transient recorder, Nature (London) **427**, 817 (2004).

[52] V. S. Yakovlev, F. Bammer, and A. Scrinzi, Attosecond streaking measurements, J. Mod. Opt. **52**, 395 (2005).

[53] M. F. Kling, J. Rauschenberger, A. J. Verhoef, E. Hasović, T. Uphues, D. B. Milošević, H. G. Muller, and M. J. J. Vrakking, Imaging of carrier-envelope phase effects in above-threshold ionization with intense few-cycle laser fields, New J. Phys. **10**, 025024 (2008).

[54] T. Rathje, N. G. Johnson, M. Möller, F. Süßmann, D. Adolph, M. Kübel, R. Kienberger, M. F. Kling, G. G. Paulus, and A. M. Sayler, Review of attosecond resolved measurement and control via carrier-envelope phase tagging with above-threshold ionization, J. Phys. B: At. Mol. Opt. Phys. **45**, 074003 (2012).

[55] A. Jašarević, E. Hasović, R. Kopold, W. Becker, and D. B. Milošević, Application of the saddle-point method to strong-laser-field ionization, J. Phys. A: Math. Theor. **53**, 125201 (2020).

[56] D. B. Milošević and W. Becker, High-order harmonic generation by bi-elliptical orthogonally polarized two-color fields, Phys. Rev. A **102**, 023107 (2020).

[57] D. Habibović, A. Gazibegović-Busuladžić, M. Busuladžić, and D. B. Milošević, Characteristics of the molecular above-threshold ionization by a bichromatic elliptically polarized field

with co-rotating components, J. Phys. B: At. Mol. Opt. Phys. **55**, 085601 (2022).

[58] B. Wolter, M. G. Pullen, M. Baudisch, M. Sclafani, M. Hemmer, A. Senftleben, C. D. Schröter, J. Ullrich, R. Moshammer, and J. Biegert, Strong-Field Physics with Mid-IR Fields, Phys. Rev. X **5**, 021034 (2015).

[59] B. Wolter, M. G. Pullen, A.-T. Le, M. Baudisch, K. Doblhoff-Dier, A. Senftleben, M. Hemmer, C. D. Schröter, J. Ullrich, T. Pfeifer, R. Moshammer, S. Gräfe, O. Vendrell, C. D. Lin, and J. Biegert, Ultrafast electron diffraction imaging of bond breaking in di-ionized acetylene, Science **354**, 308 (2016).

[60] A. S. Johnson, D. R. Austin, D. A. Wood, C. Brahms, A. Gregory, K. B. Holzner, S. Jarosch, E. W. Larsen, S. Parker, C. S. Strünber, P. Ye, J. W. G. Tisch, and J. P. Marangos, High-flux soft x-ray harmonic generation from ionization-shaped few-cycle laser pulses, Sci. Adv. **4**, eaar3761 (2018).

[61] T. Feng, A. Heilmann, M. Bock, L. Ehrentraut, T. Witting, H. Yu, H. Stiel, S. Eisebitt, and M. Schnürer, 27W 2.1 μm OPCPA system for coherent soft x-ray generation operating at 10 kHz, Opt. Express **28**, 8724 (2020).

[62] I. Powis, Photoelectron circular dichroism in chiral molecules, in *Advances in Chemical Physics* (Wiley, New York, 2008), Vol. 138, p. 267.